Structural basis for inhibition of the cyclin-dependent kinase Cdk6 by the tumour suppressor p16^{INK4a}

Alicia A. Russo*, Lily Tong†, Jie-Oh Lee†, Philip D. Jeffrey* & Nikola P. Pavletich†

** Cellular Biochemistry and Biophysics Program and † Howard Hughes Medical Institute, Memorial Sloan-Kettering Cancer Center, New York, New York 10021, USA*

The cyclin-dependent kinases 4 and 6 (Cdk4/6) that control the G1 phase of the cell cycle and their inhibitor, the p16^{INK4a} tumour suppressor, have a central role in cell proliferation and in tumorigenesis. The structures of Cdk6 bound to p16^{INK4a} and to the related p19^{INK4d} reveal that the INK4 inhibitors bind next to the ATP-binding site of the catalytic cleft, opposite where the activating cyclin subunit binds. They prevent cyclin binding indirectly by causing structural changes that propagate to the cyclin-binding site. The INK4 inhibitors also distort the kinase catalytic cleft and interfere with ATP binding, which explains how they can inhibit the preassembled Cdk4/6–cyclin D complexes as well. Tumour-derived mutations in INK4a and Cdk4 map to interface contacts, solidifying the role of CDK binding and inhibition in the tumour suppressor activity of p16^{INK4a}.

A common event in tumorigenesis is the deregulation of the eukaryotic cell cycle at the G1–S transition point, when the commitment to complete the cell cycle is made. So prevalent is this event that the vast majority of cancer cases have alterations in at least one of the main regulators of this transition[1,2]. These include the retinoblastoma (Rb) tumour suppressor, which blocks the G1–S transition[3]; the cyclin-dependent kinases 4 and 6 (Cdk4/6), which drive G1 progression and phosphorylate and inactivate Rb[4]; the cyclin D oncoprotein, which activates Cdk4/6 (ref. 5); and the p16^{INK4a} tumour suppressor, which inhibits Cdk4/6 (ref. 6).

Alterations to p16^{INK4a} in cancer are particularly common[2,7,8], occurring in ~80% of cases with certain tumour types[9]. They can either be inherited, as in familial melanoma[10,11], or occur somatically in sporadic tumours[9]. Solidifying its role in tumorigenesis, deletion of p16^{INK4a} in mice results in the development of spontaneous tumours at a young age, and high sensitivity to carcinogenic treatments[12].

Central to the tumour-suppressor effects of p16^{INK4a} is its ability to arrest cell growth at G1 by binding to and inhibiting Cdk4/6 (refs 6, 13). Tumour-derived p16^{INK4a} mutants, which lack the ability to arrest cell growth at G1 and revert cell transformation by activated oncogenes[14], are also defective in Cdk4/6 binding and inhibition[13,15–19]. Similarly, a Cdk4 mutant isolated from familial melanoma is refractory to p16^{INK4a} binding and inhibition and retains the ability to phosphorylate Rb[20,21].

p16^{INK4a} is the prototype of a family of Cdk inhibitors, specific for Cdk4/6, that also includes p15^{INK4b} (ref. 22), p18^{INK4c} (ref. 23) and p19^{INK4d} (refs 23, 24). Most observations suggest that these inhibitors act by blocking the association of Cdk4/6 with cyclin D, thus preventing the activation of the kinase. For example, in cells with high levels of endogenous p16^{INK4a}, Cdk4 is associated only with p16^{INK4a} and not with cyclin D (refs 23, 25–27); and in assembly reactions, p16^{INK4a} prevents the binding of Cdk4/6 to cyclin D (refs 24, 27, 28). *In vitro*, however, p16^{INK4a} can bind to and inhibit the preassembled Cdk4/6–cyclin D complex without dissociating cyclin D (refs 6, 13, 23), pointing to a multi-pronged mechanism

Table 1 Statistics from the crystallographic analysis

	p16^{INK4a}–Cdk6						p19^{INK4d}–Cdk6
Data set	Native	Hg λ_1	Hg λ_2	Hg λ_3	Au	Hg + Au	Native
Wavelength (Å)	0.9080	1.0093	1.0060	0.9959	0.9080	0.9080	1.0060
Beam line	CHESS A1	NSLS-X4a	NSLS-X4a	NSLS-X4a	CHESS A1	CHESS A1	NSLS-X4a
Resolution (Å)	3.4	3.9	3.9	3.9	4.0	3.8	2.8
Observations	68633	52515	51741	51960	22733	23460	88741
Unique reflections	12443	8629	8553	8553	7594	8394	33400
Data coverage (%)	97.7	97.9	98.1	97.9	96.8	89.5	96.9
R_{sym} (%)	6.8	7.1	7.4	7.6	6.6	8.7	5.5
MIR/MAD analysis:							
Phasing power	–	1.8	1.9	1.9	1.0	2.2	–
R_{cullis}	–	0.64	0.63	0.62	0.85	0.58	–
Anomalous R_{cullis}	–	0.89	0.86	0.88	–	–	–

Refinement statistics:

						R.m.s. deviations		
	Resolution (Å)	Reflections ($\|F\| > 1\sigma$)	Protein atoms	*R*-factor (%)	*R*-free (%)	Bonds (Å)	Angles (°)	*B*-factor (Å^2)
p16^{INK4a}–Cdk6	10.0–3.4	11109	3311	22.7	33.0	0.012	1.9	–
p19^{INK4d}–Cdk6	10.0–2.8	27794	3397*	25.5	30.8	0.017	2.1	3.8

* Strict non-crystallographic symmetry was used throughout refinement; the number of atoms corresponds to only one of the two complexes in the asymmetric unit.
$R_{sym} = \Sigma_h \Sigma_i |I_{hi} - I_h| / \Sigma_h \Sigma_i I_{hi}$ for the intensity (I) of i observations of reflection h. Phasing power $= \langle F_\lambda \rangle / E$, where $\langle F_\lambda \rangle$ is the r.m.s. heavy-atom structure factor and E is the residual lack of closure error. R_{cullis} is the mean residual lack of closure error divided by the dispersive or anomalous difference. Figure of merit $= |F(hkl)_{best}| / F(hkl)$. *R*-factor $= \Sigma |F_{obs} - F_{calc}| / \Sigma |F_{obs}|$, where F_{obs} and F_{calc} are the observed and calculated structure factors, respectively. *R*-free = *R*-factor calculated using 5% of the reflection data chosen randomly and omitted from the start of refinement. R.m.s. deviations are deviations from ideal geometry and root mean square variation in the *B*-factor of bonded atoms.

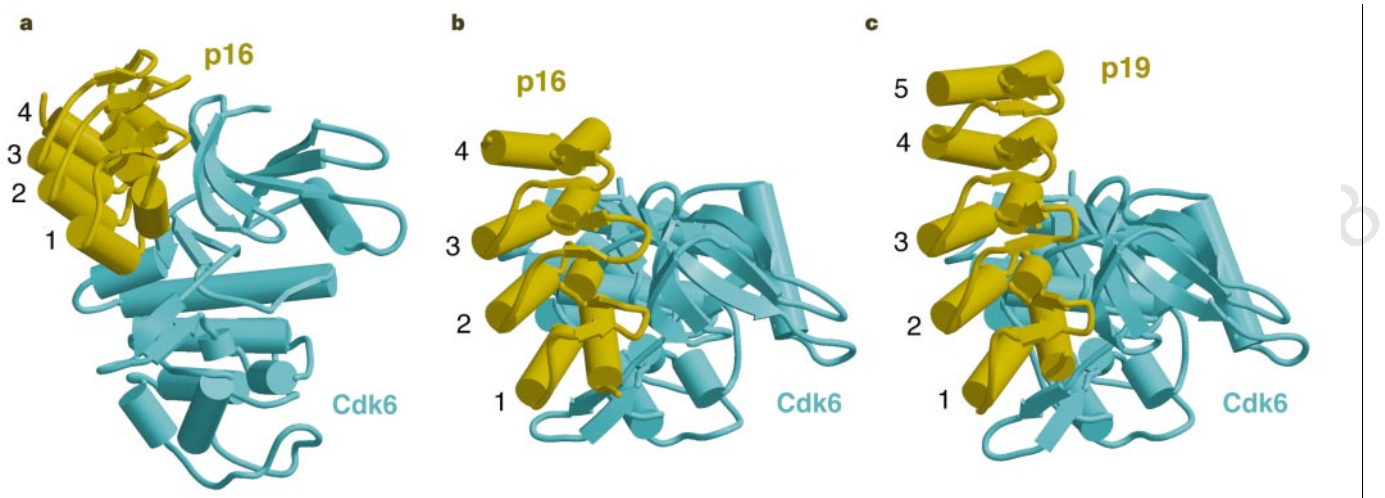

Figure 1 The INK4 inhibitors bind to one side of the catalytic cleft of Cdk6, and interact with both the N and C lobes. **a**, **b**, Schematic representation of the p16–Cdk6 complex in two orthogonal views, with the ankyrin repeats numbered. **c**, View of the p19–Cdk6 complex in an orientation equivalent to that in **b**. Figures were made with the programs MOLSCRIPT[50] and RASTER3D[51].

of action. These observations distinguish the INK4 family from the Kip/Cip family of CDK inhibitors, which have a broader CDK preference, bind the combined CDK–cyclin complex, and inhibit in part by blocking ATP binding[29].

The structures of the Cdk6–p16^{INK4a} and Cdk6–p19^{INK4d} complexes, reported here (Table 1), reveal major structural distortions in the cyclin-binding site as well as the ATP-binding site of Cdk6. These structural features help to explain how the INK4 inhibitors can block both the CDK activation process as well as the preactivated Cdk4/6–cyclin D complex.

Overall structure of the complex

The overall structure of p16-bound Cdk6 consists of an amino-terminal lobe rich in β-sheet (N lobe, residues 1–103), a larger α-helical carboxy-terminal lobe (C lobe, residues 104–301) and a catalytic cleft at the junction of the two lobes (Fig. 1a). In this general respect, p16-bound Cdk6 is similar to Cdk2 (50% sequence identity[30]), and to other eukaryotic protein kinases[31].

p16^{INK4a} (henceforth p16) and p19^{INK4d} (henceforth p19) consist of four and five ankyrin repeats, respectively. This ~30 amino acid structural motif, present in diverse proteins, has a structure that resembles the letter 'L' (ref. 32) with a pair of antiparallel helices forming the stem and a β-hairpin forming the base. As seen in the structures of monomeric p19 (ref. 33), p16 (ref. 34), and p18^{INK4c} (ref. 35), the L-like repeats stack to give an extended concave surface (Fig. 1a–c). Cdk6-bound p16 and p19 have very similar structures (1.0 Å r.m.s. deviation in Cα positions), and they do not change significantly upon binding to Cdk6 as indicated by an r.m.s. deviation of 1.3 Å in Cα positions between Cdk6-bound p16 and free p18 (ref. 35).

p16 binds to one side of the catalytic cleft, opposite where the cyclin would bind, and interacts with both the N and C lobes of Cdk6. The concave surface of p16 binds the N-lobe β-sheet, and the tips of the ankyrin repeats interact with the C lobe (Fig. 1a, b). Binding and recognition are mediated primarily by hydrogen-bond networks, with several of the residues that participate in these interactions being mutated in cancer (Figs 2, 3).

At the simplest level, p16-bound Cdk6 is inactive because it is not bound to a cyclin and is not phosphorylated. Previous structural studies of Cdk2 have shown that cyclin binding and phosphorylation are necessary to bring about activating conformational changes in two regulatory elements of the kinase[30,36,37]: the PSTAIRE helix, pushed by the cyclin, has to move into the catalytic cleft to bring in and realign active site residues[30,36]; and the T loop has to undergo successive conformational changes, first upon cyclin binding[30,36], and then upon phosphorylation[37], to relieve the blockage of the catalytic cleft and to organize the polypeptide substrate-binding site.

Like inactive free Cdk2 (ref. 30), p16-bound Cdk6 does not have any of these activating changes; unlike free Cdk2, however, p16-bound Cdk6 has structural distortions that move it further away from the active structure. Pushed apart by p16, the N and C lobes of Cdk6 are twisted away from each other, distorting the cyclin-binding site and blocking the translocation of the PSTAIRE helix into the catalytic cleft (Fig. 4a, b). The ATP-binding site is distorted

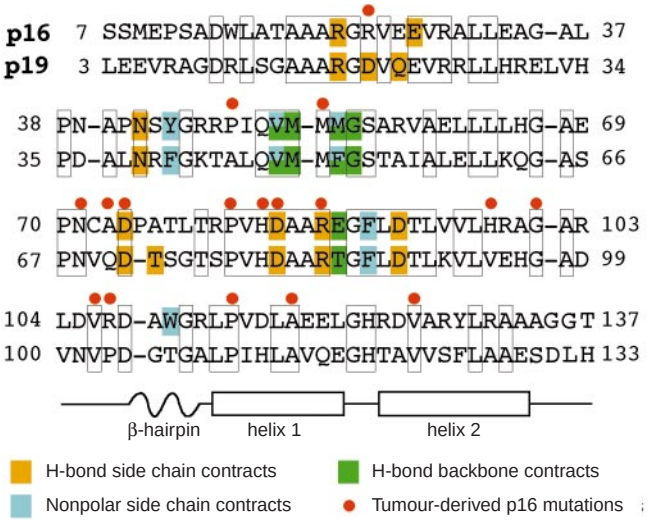

Figure 2 p16 and p19 use conserved regions to make overall conserved contacts with Cdk6. The four ankyrin repeats of p16 are aligned with the corresponding regions of p19 (the fifth p19 repeat is not shown). The ankyrin repeats have conserved secondary structure elements, except for the second ankyrin repeats of both p16 and p19, which have only one turn of helix 1. Although a much larger number of tumour-derived p16 mutants are known, those whose loss of function has not been determined are not shown. Among the differences in the p16–Cdk6 and p19–Cdk6 contacts, one involves Trp 110 of the fourth p16 repeat contacting a Cdk6 loop (Gly 36 nd Gly 37); in the p19 complex, the corresponding residue is a threonine that makes no contacts.

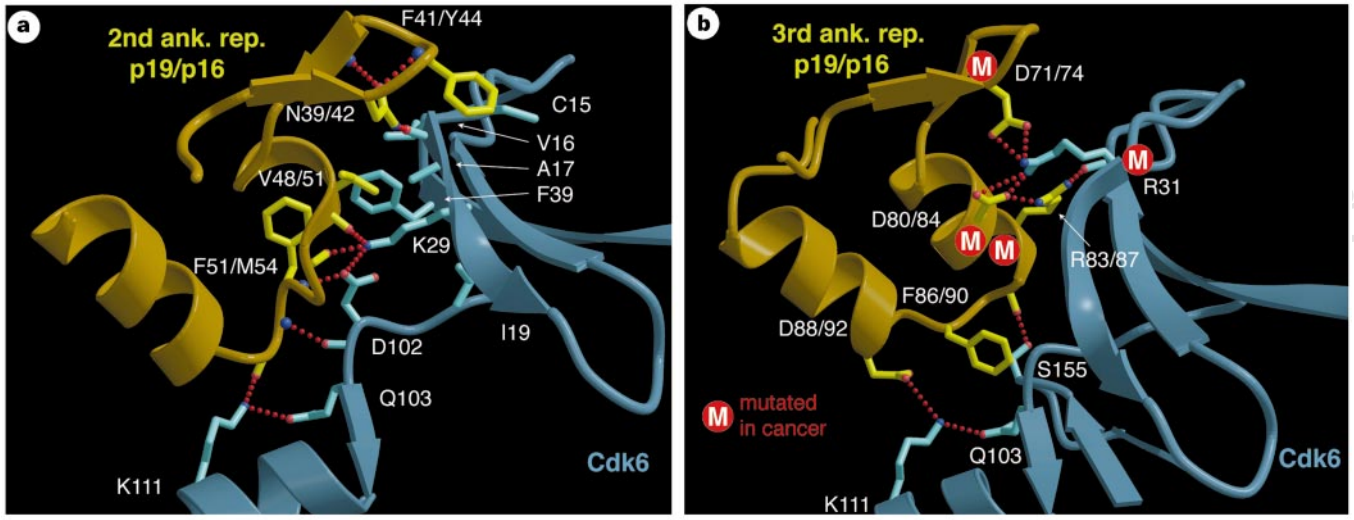

Figure 3 Conserved hydrogen-bond networks by the second and third ankyrin repeats of p16 and p19 have a central role in Cdk6 binding. **a**, Cross-section of the complex showing the contacts between Cdk6 and the second ankyrin repeat. **b**, Cross-section showing the third ankyrin repeat. Only the hydrogen-bond contacts conserved in the p16–Cdk6 and the p19–Cdk6 complexes are shown (red dotted lines). The figures show the p19–Cdk6 complex, as the atomic positions of this 2.8-Å-refined model are of higher precision than those of the 3.4-Å-refined p16–Cdk6 complex. INK4 residues are labelled first with their p19 numbers and second with their p16 numbers, separated by a slash. The secondary structure labels of Cdk6 are according to Cdk2 (ref. 30).

because of contacts from p16, which binds adjacent to the catalytic cleft, and because of the misalignment of the N and C lobes (Fig. 5a). This distortion would interfere with the productive binding of ATP, as also indicated by biochemical data in this study (Fig. 5b, c). The T loop, which seems to have significant structural freedom in CDKs, having been seen in three different places and conformations in the structures of free Cdk2 (ref. 30), cyclin A-bound Cdk2 (ref. 36), and cyclin A-bound phosphorylated Cdk2 (ref. 37), is farthest away from its expected active position, and is in the way of ATP binding as well (Fig. 6a, b).

The binding and mechanism of action of the INK4 family of CDK inhibitors is thus distinct from the Kip/Cip family of CDK inhibitors. However, it is remarkable that both families of inhibitors use the apparent structural flexibility of the kinase in their action. The Kip/Cip proteins remould the kinase N lobe, grossly changing the catalytic cleft shape[29], and the INK4 proteins both cause inhibitory structural changes and block activating structural changes.

Interactions at the interface

The p16–Cdk6 complex forms a continuous interface that buries a total of 2,200 Å^2 surface area. Roughly 60% of the buried area is contributed by interactions from the N lobe of Cdk6, with the remainder being from the C lobe. p16's most conserved second and third repeats contribute most of the interactions, whereas its first and fourth repeats make fewer interactions (Fig. 2). p19 binds similarly, except that its fourth repeat makes no significant contacts.

The binding to the N lobe is mediated by the concave surface of the four ankyrin repeats of p16, which contact the convex face of the twisted N-lobe β-sheet (β strands 1–3; Figs 1a, 3). The binding to the C lobe is mediated by the tips of the first three ankyrin repeats, which interact with the T loop (repeat 1) and with structural elements of the catalytic cleft (the α2 helix and β7–β8 strands; Figs 1a, 3).

The interface is mostly polar, relying on hydrogen-bond networks at solvent-excluded regions for binding and recognition. The interface is closely packed, as underscored by the participation of seven backbone groups, in addition to the fifteen side chain groups, in the hydrogen bond networks (Fig. 3). Most of the backbone hydrogen bonds involve the second repeat of p16, and in particular a loop (residues 52–54; Fig. 3a) that in the canonical ankyrin repeat

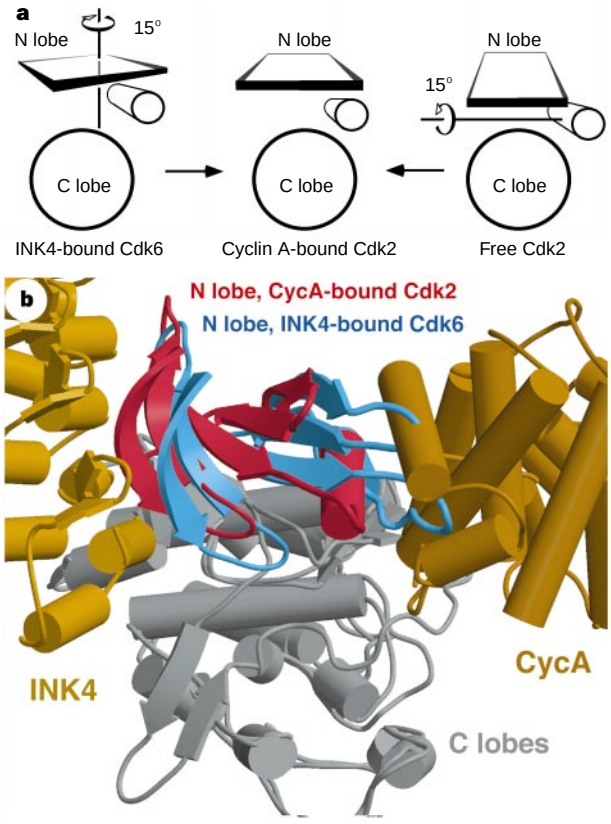

Figure 4 p16 locks the N and C lobes in a relative orientation not amenable to cyclin binding and activation. **a**, Schematic representation of the N and C lobes from p16-bound Cdk6, cyclin A-bound Cdk2 and free Cdk2. The C lobes are drawn as circles; the N-lobe β-sheets are indicated by rectangles and the PSTAIRE helices as cylinders. The axes through which rotations would bring the two lobes of p16-bound Cdk6 and of free Cdk2 into coincidence with those of the active cyclin A-bound Cdk2 are indicated. **b**, Composite figure showing the p16–Cdk6 and the cyclin A–Cdk2 complexes aligned by superimposing the C lobes of the two kinases.

structure would be an α-helix. This helix-to-loop change is a distinguishing structural feature of the INK4 family, as it is present in the structures of unbound p19 (ref. 33), p16 (ref. 34) and p18 (ref. 35) as well.

Contacts to the N and C lobes of Cdk6 are tightly coupled. For example, a hydrogen bond network of two side-chain and four backbone groups links the second ankyrin repeat of p16 to the N and C lobes of Cdk6 (centred on Lys 29 of Cdk6; Fig. 3a). Other hydrogen-bond networks link the third repeat to the N lobe (centred on Arg 31 of Cdk6; Fig. 3b), and the second and third repeats to the C lobe (centred on Lys 111 and Gln 103 of Cdk6; Fig. 3a, b). Mutation of the Cdk4 residues equivalent to Lys 29 or Arg 31 of Cdk6 abolishes p16 binding[20,38], underscoring the significance of these contacts.

Van der Waals contacts by hydrophobic residues are fewer (Figs 2, 3). One significant contact is made by the conserved Phe 90 of p16, which wedges between two loops that serve as the back wall of the catalytic cleft (residues 102–103 and 154–155 of Cdk6; Figs 3b, 5a). This contact is associated with the displacement of elements in the ATP-binding site.

Specificity for Cdk4/6. A subset of the Cdk6 residues that participate in the intermolecular hydrogen bond networks with p16 are conserved exclusively in Cdk4 and Cdk6 and are likely to be important determinants of the specificity of the INK4 family for these CDKs. Most of these residues are on the C lobe: Asp 102/Asp 97 in Cdk6 and Cdk4, respectively, are Ser/His/Ser in Cdk1, 2 and 3, respectively (Fig. 3a); Lys 111/Lys 106 are Ser/Ala/Ser (Fig. 3a, b); and Ser 155/Ser 150 are Asp/Thr/Glu (Fig. 3b). On the N lobe, the hydrogen-bonding groups (Lys 29 and Arg 31) are conserved in most CDKs, but there are several hydrophobic residues that make van der Waals contacts that show conservation correlated with INK4 specificity. The most notable residues are Ala 17/Ala 10 in Cdk6/Cdk4, which are Glu/Glu/Glu in Cdk1/2/3 respectively, and Phe 39/Phe 31, which are Val/Val/Leu (Fig. 3a).

It is likely that besides direct side chain contacts, the ability of Cdk6 to undergo conformational changes associated with p16 binding also contributes to the specificity of the INK4 proteins for this subfamily of CDKs. For example, a 10–25-residue C-terminal tail of CDKs, variable in sequence and length, is disordered in p16-bound Cdk6; in Cdk2 (ref. 30), the tail packs on a region that overlaps the p16 binding site of Cdk6.

Tumour-derived p16 and Cdk4 mutations at the interface. Solidifying the importance of CDK binding to the function of p16 as a tumour suppressor, all four of the amino acids that participate in open of the most extensive hydrogen-bond networks at the interface are mutated in cancer (Fig. 3b). This network contains Asp 74, Asp 84 and Arg 87 of p16, and Arg 31 of Cdk6, corresponding to Arg 24 of Cdk4, which is mutated in familial melanoma[20,21].

Other p16 residues that contact Cdk6 and are mutated in tumours include Glu 26 (ref. 34), which binds the T loop of Cdk6 (Fig. 2), and Asp 92 (ref. 34), which participates in another extended hydrogen-bond network with the C-lobe of Cdk6 (Fig. 3b), although these mutants have not yet been tested for loss of function.

The remaining tumour-derived missense mutations in p16 affect its structural integrity, as has been demonstrated by studies of its stability and aggregation state[17,18,34], and by the structures of free p19, p16 and p18 (refs 33–35).

p16 blocks cyclin binding indirectly

The binding of cyclin D to Cdk4/6 is likely to be similar to the binding of cyclin A to Cdk2 because the regions of cyclin A that contact Cdk2 (ref. 36) are conserved in cyclins. This is supported by

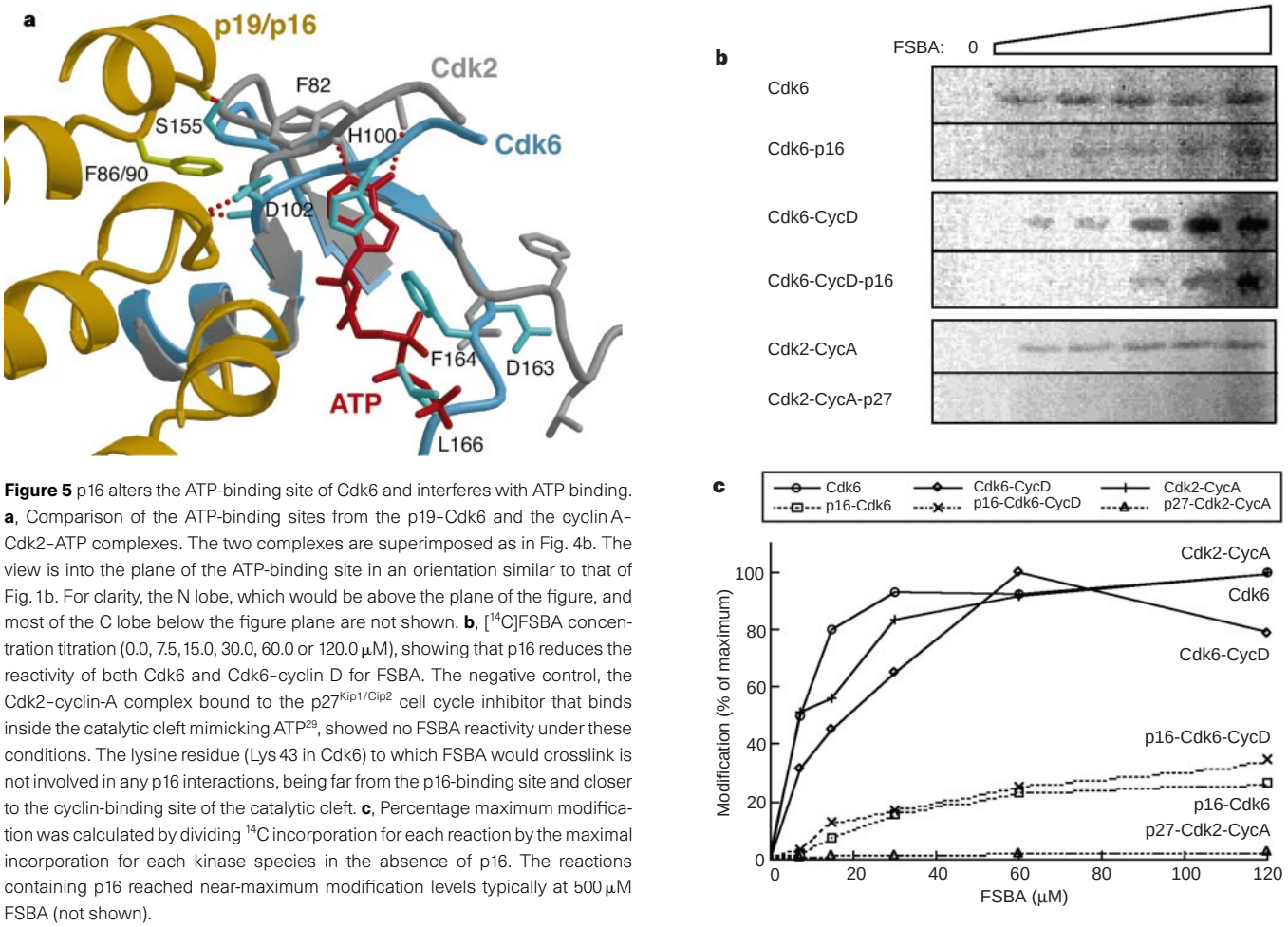

Figure 5 p16 alters the ATP-binding site of Cdk6 and interferes with ATP binding. **a**, Comparison of the ATP-binding sites from the p19–Cdk6 and the cyclin A–Cdk2–ATP complexes. The two complexes are superimposed as in Fig. 4b. The view is into the plane of the ATP-binding site in an orientation similar to that of Fig. 1b. For clarity, the N lobe, which would be above the plane of the figure, and most of the C lobe below the figure plane are not shown. **b**, [^{14}C]FSBA concentration titration (0.0, 7.5, 15.0, 30.0, 60.0 or 120.0 μM), showing that p16 reduces the reactivity of both Cdk6 and Cdk6–cyclin D for FSBA. The negative control, the Cdk2–cyclin-A complex bound to the p27$^{Kip1/Cip2}$ cell cycle inhibitor that binds inside the catalytic cleft mimicking ATP[29], showed no FSBA reactivity under these conditions. The lysine residue (Lys 43 in Cdk6) to which FSBA would crosslink is not involved in any p16 interactions, being far from the p16-binding site and closer to the cyclin-binding site of the catalytic cleft. **c**, Percentage maximum modification was calculated by dividing ^{14}C incorporation for each reaction by the maximal incorporation for each kinase species in the absence of p16. The reactions containing p16 reached near-maximum modification levels typically at 500 μM FSBA (not shown).

the ability of cyclin D to bind Cdk2 as well. In the Cdk2–cyclin A complex[36], the cyclin-binding site on the kinase consists of the β-sheet from the N lobe (15% of the CDK–cyclin interface area), the PSTAIRE helix (30%), the T loop (25%) and part of the C lobe (30%). In the p16-bound Cdk6, these structural elements differ from those of free Cdk2 or cyclin A-bound Cdk2 in their relative position or orientation. The presence of p16 would probably block some of the structural changes required for cyclin binding, and might present an activation barrier to others.

Misalignment of the N and C lobes. The relative orientations of the N and C lobes differ between p16-bound Cdk6 and cyclin A-bound Cdk2 by a 15° rotation about an axis perpendicular to the plane of the catalytic cleft (a 'vertical' axis in Fig. 4a). This axis of rotation passes through Val 76, roughly equidistant from the p16 and cyclin-binding sites, at the back of the cleft. The rotation, which is present in an identical form in the p19–Cdk6 complex, is tightly coupled to, and is probably a consequence of, the contacts that these INK4 proteins make to the two lobes (Fig. 3).

As a result of this rotation, portions of the N-lobe β-sheet at the putative cyclin-binding site undergo lateral displacements of 5–7 Å relative to the C lobe (Fig. 4b). In the presence of p16, restoration of cyclin-binding site would require structural changes to the N-lobe β-sheet. We think this is unlikely because the core of the N-lobe β-sheet is generally conserved in sequence and structure. For example, 59 of the 83 residues of the Cdk6 and Cdk2 N lobes can be superimposed with a Cα r.m.s. deviation of 1.8 Å.

This rotation about a vertical axis in the p16-bound Cdk6 lobes is unlike that which free Cdk2 undergoes upon binding to cyclin A, where the N and C lobes rotate by 15° about a horizontal axis in the plane of the catalytic cleft (Fig. 4a). This rotation of the lobes in the Cdk2–cyclin A complex results in the opening of the catalytic cleft, making room for the translocation of the PSTAIRE helix into the cleft[30,36].

PSTAIRE helix translocation blocked. In both the p16–Cdk6 and p19–Cdk6 structures the PSTAIRE helix has high temperature factors and is not well ordered, although its overall position is well determined in the maps of the p16–Cdk6 complex derived from a combination of multiple isomorphous replacement (MIR) and multi-wavelength anomalous diffraction (MAD) methods. To reconstitute the cyclin-binding site, the PSTAIRE helix will have to move into the catalytic cleft relative to the C lobe. This translocation is indirectly antagonized by p16, because the misalignment of the N and C lobes places side chains in the way (Fig. 4b).

T loop is away from the cyclin-binding site. In both the p16 and p19-bound Cdk6 structures, the T loop (residues 162–182) exits the catalytic cleft from the side where the INK4 inhibitor is bound, this being aided by its interactions with the uniquely aligned N and C lobes (Fig. 6a). This is in contrast to the Cdk2 structures, where the T loop exits the catalytic cleft closer to the cyclin-binding side (Fig. 6a). Immediately after it exits the catalytic cleft, the T loop forms a 10-residue β-hairpin, which is well ordered and rigid in the p19–Cdk6 structure (Fig. 6b), but is partly flexible in the p16–Cdk6 structure. The β-hairpin packs on the C lobe via hydrogen-bond and hydrophobic interactions, and also makes a set of hydrogen-bond contacts to p19 (Arg 168 of Cdk6 with Asp 20 and Gln 22 of p19; Fig. 2). It is remarkable that this is the fourth distinct T-loop conformation observed in CDK structures, and represents the largest displacement away from the T-loop structure observed in the fully active cyclin A-phosphorylated Cdk2 complex (with a maximal displacement of 35 Å compared to 21 Å for free Cdk2; ref. 36).

In the structure of mouse p19 bound to human Cdk6 (ref. 39), the T loop is observed in yet another conformation. It is not known which T-loop conformation is favoured in solution, as crystallization conditions, crystal packing forces and other effects can shift the equilibrium in the crystallization experiments. Nevertheless, the observed variety in T-loop conformations supports a role for the inherent flexibility of the T loop, as seen in the Cdk2 structures as well, in keeping the CDK inactive.

Distortion of the ATP-binding site

In both the p16- and p19-bound Cdk6 structures, an internal catalytic cleft loop (residues 99–102) that would otherwise make backbone hydrogen bonds to the N6 and N1 groups of the ATP purine[36] is dislodged by an average of 2.5 Å by direct contacts from p16 (Fig. 5a). N- and C-lobe side chains that would contact the ATP purine and phosphate groups as seen in the Cdk2 structures[30,36] are partly out of register owing to the misalignment of the two lobes. In addition, side chains from the dislodged internal catalytic cleft loop (His 100) and from the T loop (Phe 164 and Leu 166) as it exits from the cleft have invaded portions of the space where the ATP purine, sugar and phosphate groups would be (Fig. 5a). These features of the catalytic cleft would not entirely preclude ATP from binding the way the Kip/Cip family of inhibitors do, as there is room remaining, especially if some side chains twist out of the way. But they would reduce the affinity of the kinase for ATP, and could well misorient any bound ATP with respect to catalysis. This is supported by binding studies of the ATP analogue FSBA (*p*-fluorosulphonylbenzoyl 5′-adenosine), which crosslinks covalently to an active-site lysine residue conserved in protein kinases[40,41]. Figure 5b and c

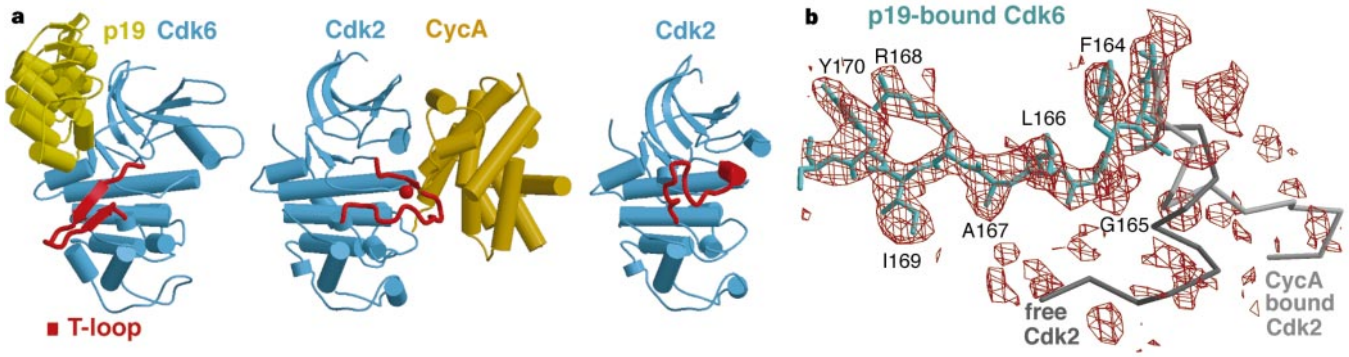

Figure 6 The T loop has large displacements from the active conformation compared to Cdk2 structures. **a**, Comparison of the three structures oriented by their C lobes highlights the different conformations and positions of their T loops. Equivalent portions of the T loops between the conserved DFG and APE sequences are shown in red. The red sphere in cyclin-A-bound Cdk2 indicates the phosphate group on the Thr 160 of that kinase. **b**, Omit difference electron density of the p19–Cdk6 complex showing the portion of the T loop as it exits form the catalytic cleft and the first strand fo the β-hairpin (the second strand is below the plane of the figure). Model bias was removed by omitting the T loop (residues 162–184) and by subjecting the model to simulated annealing refinement from 4,000 K with ncs-strict in X-PLOR. The map was averaged iteratively with the program RAVE[48], and the resulting phases were used to construct the $F_o - F_c$ omit map. Only difference density in the vicinity of the T-loop atoms (including side-chain atoms from the two Cdk2 T loops) is shown. The map is contoured at 2.0 σ.

shows that p16 binding reduces the reactivity of Cdk6 for FSBA by a factor of ~20.

Inhibition of the Cdk4/6–cyclin-D complex by p16

It is not yet clear whether the structure of the kinase in the ternary p16–Cdk4/6–cyclin D complex[6,13,23] would be closer to that of p16-bound Cdk6 or cyclin-A-bound Cdk2. Nevertheless, the p16–Cdk6–cyclin D complex has FSBA reactivity that is ~20-fold lower than that of the Cdk6–cyclin D complex (Fig. 5b, c). This indicates that when p16 is bound to the Cdk6–cyclin D complex, at least some of the distortions in the ATP-binding site are present and contribute to the inhibition of the Cdk6–cyclin D complex by p16.

One model for the binding of p16 to Cdk6–cyclin D is that p16 might still make most of the N-lobe contacts, as it has some detectable affinity for the isolated N lobe[34]. This might be sufficient to bring about some of the changes in the ATP-binding site. This model is consistent with the report of a 20-residue p16 peptide with residual Cdk4 binding and inhibitory activity[42]. This peptide encompasses the residues that form the hydrogen-bond network with Arg 31 of the N lobe of Cdk6, which could serve as an initial binding point (Fig. 3b), and it also contains the Phe 90 residue, which has a central role in the dislocation of the ATP-interacting loop in the catalytic cleft (Figs 3b, 5a).

Implications for other Cdk4/6 complexes

The structural distortions seen in p16-bound Cdk6 raise the possibility that other macromolecular complexes of Cdk6 might also be antagnonized by INK4 binding. We tested Cdc37, which might be required for Cdk–cyclin association in yeast[43] and might stabilize Cdk4 in mammalian cells[44]. Binding studies *in vitro* with purified proteins (not shown) indicate that p16 both can block Cdc37 binding to Cdk6 and also can dissociate prebound Cdc37–Cdk6 complexes.

INK4 proteins also inhibit the binding of the Kip/Cip family of inhibitors to Cdk4/6 (ref. 45). The structure reveals that the two families of inhibitors have partly overlapping binding sites on the CDK (ref. 29).

Structural flexibility in CDK regulation

CDKs are among the most extensively and diversely regulated eukaryotic protein kinases, as they have to respond to a multitude of growth regulatory pathways that converge on the cell cycle. Structural studies of Cdk2 activation by cyclin A (ref. 36) and by phosphorylation[37], and of inhibition by $p27^{Kip1/Cip2}$ (ref. 29) have revealed that all of these processes are associated with conformational changes. The structures of the p16–Cdk6 and p19–Cdk6 complexes strongly reinforce the concept that cyclin-dependent kinases possess an inherent structural flexibility that is central to their regulation. □

Methods

Protein overexpression and purification. Human Cdk6 (ref. 46) was overexpressed using a baculovirus vector in Hi5 (Invitrogen) insect cells grown in suspension in serum-free media (Sf900, Gibco). It was purified by affinity chromatography using a column of human p16, prepared as a glutathione *S*-transferase (GST)-p16 fusion in *Escherichia coli*. The affinity-purified GST–p16–Cdk6 complex was treated with thrombin at 4 °C to cleave the GST fusion protein, and was further purified by anion-exchange and gel-filtration chromatography. The complex was concentrated by ultrafiltration to typically 50 mg ml^{-1} in a buffer of 25 mM Tris-HCl, 200 mM NaCl, 5 mM dithiothreitol (DTT), pH 7.5. The complex of human p19 bound to Cdk6 was prepared similarly, and was concentrated to 35 mg ml^{-1}. The overexpressed Cdk6 had a mass consistent with *N*-acetylation and lack of phosphorylation.

For the biochemical studies, Cdk6 was overexpressed as a GST–Cdk6 fusion protein in insect cells. After cleavage from the GST, Cdk6 was purified by anion-exchange and gel-filtration chromatographies in the same buffer as the p16–Cdk6 complex. The Cdk6–cyclin D complex was prepared by co-infecting insect cells with separate baculoviruses expressing GST–Cdk6 and cyclin D1, then isolating, purifying and cleaving the GST–Cdk6–cyclin D complex as with free Cdk6. After cleavage from GST, free Cdk6, which was in large excess, was separated from the Cdk6–cyclin D complex by anion-exchange and gel-filtration chromatographies.

Crystallization and data collection. Crystals of the p16–Cdk6 complex were grown at 4 °C by the hanging-drop vapour-diffusion method, from 11% isopropanol, 40 mM Hepes-Na, 5 mM DTT, pH 7.5. They form in space group $P4_122$ with $a = b = 123.4$ Å, $c = 114.6$ Å and contain one complex in the asymmetric unit. Heavy-atom soaks were performed in crystallization buffer lacking DTT with 0.4 mM thimerosal for 4 h, or 1 mM $K_2Au(CN)_4$ for 2 h, or 0.1 mM thimerosal and 2 mM $K_2Au(CN)_4$ for 4 h. Diffraction data were collected with crystals flash-frozen in crystallization buffer supplemented with 25% PEG400 at −170 °C.

Crystals of the p19–Cdk6 complex were grown from 26% saturated $(NH_4)_2(SO_4)$, 8–12% dioxane, 100 mM MES-Na, 5 mM DTT, pH 6.5. They form in space group *C*2 with $a = 98.4$, $b = 116.8$, $c = 132.2$ Å, $\beta = 110.4°$ and have two complexes in the asymmetric unit. The crystals were pretreated with glutaraldehyde (diffused into the drop form a reservoir of 30% glutaraldehyde) to reduce their tendency to crack and lose diffraction along b^* and c^*. They were then harvested in 30% saturated $(NH_4)_2(SO_4)$, 10% dioxane, 100 mM MES-Na, 5 mM DTT, pH 6.5, supplemented with 20% glycerol just before flash freezing at −170 °C. Diffraction was strongly anisotropic, extending to 2.1 Å along a^*, compared to only ~3 Å along c^*.

Structure determination and refinement. The structure of the p16–Cdk6 complex was determined by a combination of MIR and MAD. Initial phases (mean figure of merit of 0.72) were calculated at 3.8 Å resolution with the program MLPHARE[47] and were improved by density modification with the program DM[47]. A model of Cdk6 derived from the structure of Cdk2, and a model of p16 derived from the structure of p18 were readily built into the MIR/MAD maps with the program O (ref. 48). The model was refined with the programs X-PLOR[49] and REFMAC[47] to 3.4 Å. The refinement included the MIR/MAD phases as additional restraints, solvent correction, and grouped B factors (two per residue). The final model contains residues 10–134 of p16, and 10–48 and 57–301 of Cdk6. Residues 48–72 and 167–181 have high temperature factors; we presume they are partly disordered.

The structure of the p19–Cdk6 complex was determined by molecular replacement using the p16–Cdk6 structure as the search model. Anisotropic *B* factor refinement with X-PLOR resulted in a large correction to the data ($B_{11} = -29.0$, $B_{22} = -8.0$, $B_{33} = 37.0$, $B_{13} = 17.9$ Å^2), which significantly improved the free *R*. The initial $2F_o - F_c$ maps were averaged iteratively with the program RAVE[48] to a correlation coefficient of 0.78. Throughout refinement the two complexes in the asymmetric unit were kept identical by applying strict non-crystallographic symmetry (ncs) in X-PLOR, as there was no evidence of significant positional differences between the two complexes when the strict-ncs constraints were removed. After restrained temperature factor refinement, simulated annealing omit maps (X-PLOR) averaged by RAVE were used to confirm every part of the complex systematically. Solvent correction was applied with X-PLOR. The final model contains residues 6–160 of p19, and residues 11–48, 57–87 and 92–301 of Cdk6, and has no water molecules.

Labelling with [^{14}C]FSBA. Reactions, performed in accordance with published procedures[41], contained 10.0 μM protein, 50 mM NaCl, 25 mM Hepes-Na, pH 7.5, [^{14}C]FSBA (5′-*p*-[adenine-8-^{14}C]fluorosulphonylbenzoyl adenosine; NEN–Du Pont), and 10% DMSO (from the added FSBA), were incubated at 30.0 °C for 15 min, then resolved by SDS–PAGE. The gels were dried without fixing, exposed to a phosphorimager plate, and ^{14}C incorporation was quantitated by integration of the bands with background correction. For each kinase species, the reactions with and without p16 were done simultaneously and were repeated at least twice.

Received 15 May; accepted 10 July 1998.

1. Sherr, C. J. Cancer cell cycles. *Science* **274,** 1672–1677 (1996).
2. Hall, M. & Peters, G. Genetic alterations of cyclin, cyclin-dependent kinases, and cdk inhibitors in human cancer. *Adv. Cancer Res.* **68,** 68–108 (1996).
3. Weinber, R. A. The retinoblastoma protein and cell cycle control. *Cell* **81,** 323–330 (1995).
4. Sherr, C. J. G1 phase progression cycling on cue. *Cell* **79,** 551–555 (1994).
5. Hunter, T. & Pines, J. Cyclins and cancer II: cyclin D and cdk inhibitors come of age. *Cell* **79,** 573–582 (1994).

6. Serrano, M., Hannon, G. J. & Beach, D. A new regulatory motif in cell-cycle control causing specific inhibition of cyclin D/CDK4. *Nature* **366,** 704–707 (1993).
7. Kamb, A. *et al.* A cell cycle regulator potentially involved in genesis of many tumor types. *Science* **264,** 436–440 (1994).
8. Nobori, T. *et al.* Deletions of the cyclin-dependent kinase-4 inhibitor gene in multiple human cancers. *Nature* **368,** 753–756 (1994).
9. Caldas, C. *et al.* Frequent somatic mutations and homozygous deletions of the p16 (MTS1) gene in pancreatic adenocarcinoma. *Nature Genet.* **8,** 27–32 (1994).
10. Hussussian, C. J. *et al.* Germline p16 mutations in familial melanoma. *Nature Genet.* **8,** 15–21 (1994).
11. Kamb, A. *et al.* Analysis of the p16 gene (CDKN2) as a candidate for the chromosome 9p melanoma susceptibility locus. *Nature Genet.* **8,** 23–26 (1994).
12. Serrano, M. *et al.* Role of the INK4a locus in tumor suppression and cell mortality. *Cell* **85,** 27–37 (1996).
13. Koh, J., Enders, G. H., Dynlacht, B. D. & Harlow, E. Tumour-derived p16 alleles encoding proteins defective in cell-cycle inhibition. *Nature* **375,** 506–510 (1995).
14. Serrano, M., Gomez-Lahoz, E., DePinho, R. A., Beach, D. & Bar-Sagi, D. Inhibition of ras-induced proliferation and cellular transformation by p16INK4. *Science* **267,** 249–252 (1995).
15. Yang, R., Gombart, A. F., Serrano, M. & Koeffler, H. P. Mutational effects on the p16INK4a tumor supressor protein. *Cancer Res.* **55,** 2503–2506 (1995).
16. Ranade, K. *et al.* Mutations associated with familial melanoma impair p16INK4 function. *Nature Genet.* **10,** 114–116 (1995).
17. Parry, D. & Peters, G. Temperature-sensitive mutants of $p16^{CDKN2}$ associated with familial melanoma. *Mol. Cell. Biol.* **16,** 3844–3852 (1996).
18. Zhang, B. & Peng, Z. Defective folding of mutant p16(INK4) proteins encoded by tumor-derived alleles. *J. Biol. Chem.* **271,** 28734–28737 (1996).
19. Arap, W., Knudsen, E. S., Wang, J. Y., Cavenee, W. K. & Huang, H. J. Point mutations can inactivate in vitro and in vivo activities of p16(INK4a)/CDKN2A in human glioma. *Oncogene* **14,** 603–609 (1997).
20. Wolfel, T. *et al.* A $p16^{INK4a}$-insensitive CDK4 mutant targeted by cytolytic T lymphocytes in a human melanoma. *Science* **269,** 1281–1284 (1995).
21. Zuo, L. *et al.* Germline mutations in the $p16^{INK4a}$ binding domain of CDK4 in familial melanoma. *Nature Genet.* **12,** 97–99 (1996).
22. Hannon, G. J. & Beach, D. $p15^{INK4B}$ is a potential effector of TGF β-induced cell cycle arrest. *Nature* **371,** 257–261 (1994).
23. Hirai, H., Roussel, M. F., Kato, J. Y., Ashmun, R. A. & Sherr, C. J. Novel INK4 proteins, p19 and p18, are specific inhibitors of the cyclin D-dependent kinases CDK4 and CDK6. *Mol. Cell. Biol.* **15,** 2672–2681 (1995).
24. Guan, K. L. *et al.* Isolation and characterization of $p19^{INK4d}$, a p16-related inhibitor specific to CDK6 and CDK4. *Mol. Biol. Cell* **7,** 57–70 (1996).
25. Xiong, Y., Zhang, H. & Beach, D. Subunit rearrangement of the cyclin-dependent kinases is associated with cellular transformation. *Genes Dev.* **7,** 1572–1583 (1993).
26. Li, Y., Nichols, M. A., Shay, J. W. & Xiong, Y. Transcriptional repression of the D-type cyclin-dependent kinase inhibitor p16 by the retinoblastoma susceptibility gene product pRb. *Cancer Res.* **54,** 6078–6082 (1994).
27. Parry, D., Bates, S., Mann, D. J. & Peters, G. Lack of cyclin D–Cdk complexes in Rb-negative cells correlates with high levels of p16INK4/MTS1 tumour suppressor gene product. *EMBO J.* **14,** 503–511 (1995).
28. Lukas, J. *et al.* Retinoblastoma-protein-dependent cell-cycle inhibition by the tumour suppressor p16. *Nature* **375,** 503–506 (1995).
29. Russo, A. A., Jeffrey, P. D., Patten, A. K., Massagué, J. & Pavletich, N. P. Crystal structure of the $p27^{Kip1}$ cyclin-dependent-kinase inhibitor bound to the cyclin A–Cdk2 complex. *Nature* **382,** 325–331 (1996).
30. De Bondt, H. L. *et al.* Crystal structure of cyclin-dependent kinase 2. *Nature* **363,** 595–602 (1993).
31. Knighton, D. R. *et al.* Crystal structure of the catalytic subunit of cyclic adenosine monophosphate-dependent protein kinase. *Science* **253,** 407–413 (1991).
32. Gorina, S. & Pavletich, N. P. Structure of the p53 tumor suppressor bound to the ankyrin and SH3 domains of 53BP2. *Science* **274,** 1001–1005 (1996).
33. Luh, F. Y. *et al.* Structure of the cyclin-dependent kinase inhibitor $p19^{Ink4d}$. *Nature* **389,** 999–1003 (1997).
34. Byeon, I. *et al.* Tumor suppressor $p16^{INK4A}$: determination of solution structure and analyses of its interaction with cyclin-dependent kinase 4. *Mol. Cell* **1,** 421–431 (1998).
35. Venkataramani, R., Swaminathan, K. & Marmostein, R. Crystal structure of the CDK4/6 inhibitory protein $p18^{INK4c}$ provides insights into ankyrin-like repeat structure/function and tumor-derived $p16^{INK4}$ mutations. *Nature Struct. Biol.* **5,** 74–81 (1998).
36. Jeffrey, P. D. *et al.* Mechanism of CDK activation revealed by the structure of cyclin A–CDK2 ocmplex. *Nature* **376,** 313–320 (1995).
37. Russo, A., Jeffrey, P. D. & Pavletich, N. P. Structural basis of cyclin-dependent kinase activation by phosphorylation. *Nature Struct. Biol.* **3,** 696–700 (1996).
38. Coleman, K. G. *et al.* Identification of CDK4 sequences involved in cyclin D1 and p16 binding. *J. Biol. Chem.* **272,** 18869–18874 (1997).
39. Brotherton, D. H. *et al.* Crystal structure of the complex of the cyclin D-dependent kinase Cdk6 bound to the cell cycle inhibitor $p19^{INK4d}$. *Nature* **395,** 244–250 (1998).
40. Zoller, M. J., Nelson, N. C. & Taylor, S. S. Affinity labeling of cAMP-dependent protein kinase with p-Fluorosulfonylbenzoyl adenosine. *J. Biol. Chem.* **256,** 10837–10842 (1981).
41. Atherton-Fessler, S., Parker, L. L., Geahlen, R. L. & Piwnica-Worms, H. Mechanisms of $p34^{cdc2}$ regualtion. *Mol. Cell. Biol.* **13,** 1675–1685 (1993).
42. Fahraeus, R., Paramio, J. M., Ball, K. L., Lain, S. & Lane, D. P. Inhibition of pRb phosphorylation and cell-cycle progression by a 20-residue peptide derived from $p16^{CDKN2/INK4A}$. *Curr. Biol.* **6,** 84–91 (1996).
43. Gerber, M. R., Farrell, A., Deshaies, R. J., Herskowitz, I. & Morgan, D. O. Cdc37 is required for association of the protein kinase Cdc28 with G1 and mitotic cyclins. *Proc. Natl Acad. Sci. USA* **92,** 4651–4655 (1995).
44. Stepanova, L., Leng, X., Parker, S. B. & Harper, J. W. Mammalian p50Cdc37 is a protein kinase-targeting subunit of Hsp90 that binds and stabilizes Cdk4. *Genes Dev.* **10,** 1491–1502 (1996).
45. Reynisdottir, I., Polyak, K., Iavarone, A. & Massagué, J. Kip/Cip and Ink4 Cdk inhibitors cooperate to induce cell cycle arrest in response to TGF-beta. *Genes Dev.* **9,** 1831–1845 (1995).
46. Meyerson, M. & Harlow, E. Identification of G1 kinase activity for cdk6, a novel cyclin D partner. *Mol. Cell. Biol.* **14,** 2077–2086 (1994).
47. Collaborative Computational Project, Number 4. The CCP4 suite: programs for protein crystallography. *Acta Crystallogr. D* **50,** 760–763 (1994).
48. Jones, T. A., Zou, J.-Y., Cowan, S. W. & Kjeldgaard, M. Improved methods for building protein models in electron density maps and the location of errors in these models. *Acta Crystallogr. A* **47,** 110–119 (1991).
49. Brunger, A. T. *X-PLOR, a System for Crystallography and NMR* (Yale Univ. Press, New Haven, CT, 1991).
50. Kraulis, P. J. Molscript: a program to produce both detailed and schematic plots of protein structures. *J. Appl. Crystallogr.* **24,** 946–950 (1991).
51. Merrit, E. A. & Murphy, M. E. Raster3D Version 2.0: a program for photorealistic molecular graphics. *Acta Crystallogr. D* **50,** 869–873 (1994).

Acknowledgements. We thank S. Geromanos and H. Erdjument-Bromage of the Sloan-Kettering Microchemistry Facility for N-terminal sequence and mass spectroscopic analyses; H. Chou and E. D. Harlow for baculovirus vectors expressing Cdk6, GST–Cdk6 and cyclin D1; R. Marmorstein for the crystallographic coordinates of p18; C. Ogata of the National Synchrotron Light Source X4A beam line and the staff of the Cornell High Energy Synchrotron Source MacChess for help with data collection; and C. Murray for administrative help. Supported by the Howard Hughes Medical Institute, the NIH, the Pew Charitable Trusts, the Dewitt Wallace Foundation, and the Samuel and May Rudin Foundation.

Correspondence and requests for materials should be addressed to N.P.P. (e-mail: Nikola@xray2.mskcc.org). Coordinates have been deposited with the Brookhaven Protein Data Bank (accession codes 1BI7 and 1BI8.).